PVMirror: A New Concept for Tandem Solar Cells and Hybrid Solar Converters

Zhengshan J. Yu, Kathryn C. Fisher, Brian M. Wheelwright, Roger P. Angel, and Zachary C. Holman

***Abstract*—As the solar electricity market has matured, energy conversion efficiency and storage have joined installed system cost as significant market drivers. In response, manufacturers of flat-plate silicon photovoltaic (PV) cells have pushed cell efficiencies above 25%—nearing the 29.4% detailed-balance efficiency limit—and both solar thermal and battery storage technologies have been deployed at utility scale. This paper introduces a new tandem solar collector employing a "PVMirror" that has the potential to both increase energy conversion efficiency and provide thermal storage. A PVMirror is a concentrating mirror, spectrum splitter, and light-to-electricity converter all in one: It consists of a curved arrangement of PV cells that absorb part of the solar spectrum and reflect the remainder to their shared focus, at which a second solar converter is placed. A strength of the design is that the solar converter at the focus can be of a radically different technology than the PV cells in the PVMirror; another is that the PVMirror converts a portion of the diffuse light to electricity in addition to the direct light. We consider two case studies—a PV cell located at the focus of the PVMirror to form a four-terminal PV–PV tandem, and a thermal receiver located at the focus to form a PV–CSP (concentrating solar thermal power) tandem—and compare the outdoor energy outputs to those of competing technologies. PVMirrors can outperform (idealized) monolithic PV–PV tandems that are under concentration, and they can also generate nearly as much energy as silicon flat-plate PV while simultaneously providing the full energy storage benefit of CSP.**

***Index Terms*—Concentrating solar power, concentrator, multi-junction, photovoltaic cells, solar energy, solar thermal, tandem.**

I. Introduction

MODULE efficiency is the primary cost driver in the flat-plate photovoltaic (PV) industry because the module cost now accounts for less than half of the total installed system cost [1], [2]. Consequently, in the past five years, commercial cell and module efficiencies have improved dramatically: In 2014, Panasonic announced a large-area 25.6%-efficient silicon heterojunction cell that broke the 14-year-old record for crystalline silicon [3], and SunPower produced a 25%-efficient interdigitated-back-contact silicon cell on a manufacturing line [4]. These devices are approaching the 29.43% theoretical efficiency limit of a silicon PV cell, as reassessed by Richter *et al.* in 2012 [5], and are unlikely to exceed 26% as predicted by Swanson in 2005 and re-evaluated by Smith *et al.* in 2014 [4]. The recent efficiency gains are not limited to silicon; Alta Devices reported a record 28.8%-efficient single-junction cell based on its GaAs technology in 2011 [6]. This device is not far off the 33% detailed-balance radiative limit for a single-junction PV cell with the ideal bandgap of 1.1–1.4 eV [7], [8]. Evidently, regardless of technology, single-junction PV cells are nearing their terminal efficiency plateau. What, then, is the next step for PV? Though many approaches have been proposed to surpass the single-junction limit [9], [10], only multi-junction devices have proven successful thus far.

Theoretical analysis shows that by choosing proper materials with 36 different bandgaps, the efficiency of a multi-junction PV cell can be as high as 72% [11]. The most developed embodiment of multi-junction PV cells is that of a monolithically integrated two-terminal device in which wider-bandgap cells are stacked directly on top of narrower-bandgap cells, separated by recombination junctions. With three or four junctions of III–V materials arranged in this structure, several groups have successfully produced PV cells that exceed 40% efficiency under concentration [12]–[15]. However, due to the expense of the epitaxial growth substrate, III–V precursors, and growth machines, these cells are restricted to high-concentration (and space) applications where their cost is discounted by the concentration ratio. The penalty of high concentration—in addition to the cost of tracking—is the loss of all diffuse light, which accounts for 25% of annual solar energy even in places as sunny as Phoenix [16]. To reach high efficiencies with respect to the global incident spectrum, it would be nice to reproduce the success of III–V multi-junctions in the much larger flat-plate and low-concentration markets using cheaper materials and growth techniques, as was attempted with thin-film silicon PV [17]. Unfortunately, current mismatch, lattice mismatch, and processing compatibility severely limit material choice and device design.

All multi-junction PV cells split the solar spectrum and send to each sub-cell the wavelengths that it may best use (those above, but near, the absorber bandgap). The monolithically integrated multi-junction cells just discussed (as well as four-terminal stacked cells) achieve this separation through absorptive filtering in which narrow-bandgap cells are illuminated only with light not absorbed by the wide-bandgap cells above. There are, however, four other options to split the spectrum: reflective filtering, refractive filtering, holographic filtering, and luminescent filtering (see Imenes and Mills for a review [18]). These "optically coupled" multi-junction cells have the advantage that

Manuscript received April 17, 2015; revised June 1, 2015; accepted July 16, 2015. Date of publication August 25, 2015; date of current version October 19, 2015. The information, data, or work presented herein was funded in part by the Advanced Research Projects Agency-Energy (ARPA-E), U.S. Department of Energy, under Award Number DE-AR0000474.

Z. J. Yu, K. C. Fisher, and Z. C. Holman are with the School of Electrical, Computer, and Energy Engineering, Arizona State University, Tempe, AZ 85281 USA (e-mail: zhengshan.j.yu@asu.edu; kathryn.fisher@asu.edu; zachary.holman@asu.edu).

B. M. Wheelwright and R. P. Angel are with the College of Optical Sciences, University of Arizona, Tucson, AZ 85721 USA (e-mail: bmw4@email.arizona.edu; angelj@email.arizona.edu).

Color versions of one or more of the figures in this paper are available online at http://ieeexplore.ieee.org.

Digital Object Identifier 10.1109/JPHOTOV.2015.2458571

current mismatch and cell compatibility are non-issues, but they have traditionally faced other challenges. The reflective method uses a dichroic mirror (also called a Bragg reflector), which is made by stacking high- and low-refractive-index dielectric layers to transmit only certain bands of light; the rest are reflected. Moon *et al.* reported an outdoor efficiency of 28.5% under 165 suns with two separate PV cells, made of silicon and AlGaAs, coupled with a dichroic mirror [19]. Recently, with a four-junction receiver, Mitchell *et al*. demonstrated 34% efficiency under one-sun (non-concentrated) outdoor illumination, but the cells were made of III–V materials and arranged such that the cell area was much larger than the aperture area, so, economical operation is expected only under high concentration [20]. The refractive method uses a prism to disperse sunlight to PV cells with different bandgaps spaced laterally, but collimated light is required in order to prevent overlap of spectral bands. The advantage of holographic filtering is that the incident spectrum can be simultaneously concentrated and split with a single optical element, but sufficiently high diffraction efficiencies have yet to be demonstrated, and the foci of the beams tend to fall on a curved surface rather than a plane [21], [22]. Luminescent filtering requires a dye with a high photoluminescence quantum yield and a Stokes shift that is large enough to prevent reabsorption of emitted light, but not so large that a substantial fraction of the photon energy is thrown away in the downshift [23], [24].

Here we propose a new two-junction or tandem concept that employs absorptive or reflective filtering to optically couple the sub-cells. This "PVMirror" technology utilizes PV cells as a three-in-one technology—they act as a concentrating mirror, spectrum splitter, and high-efficiency light-to-electricity converter. Distinct from high-concentration multi-junctions, PVMirrors convert part of the diffuse spectrum in addition to the direct beam and can be used to couple two PV cells of wildly different technologies or even one PV cell and a non-PV solar energy converter. Two case studies are presented that show performance improvement with the application of PVMirrors.

II. The PVMirror Concept

A PVMirror uses a one-sun PV cell to split the solar spectrum and reflect light that is not absorbed. This can be achieved with a wide-bandgap cell in which the absorber's bandgap acts as the splitting edge. The same function is provided by the top cell in a stacked tandem, but in a PVMirror a specular rear reflector is employed so sub-bandgap light is reflected out the front of the cell rather than transmitted. Alternatively, a PVMirror can be made using reflective instead of absorptive filtering by putting a spectrum-splitting dichroic mirror on top of the PV cell, which can then have any bandgap, surface morphology, and rear reflector. In either case, by arranging the PV cells so that the specularly reflected light from many cells arrives at a common focus—as with a trough, dish, Fresnel mirror, or heliostat field—the resulting concentrated light can be used to illuminate another PV cell, power a thermal cycle, or drive any other solar energy converter.

There are three main embodiments of PVMirrors. They are shown in Fig. 1 for a PV–PV tandem in the trough geometry. The

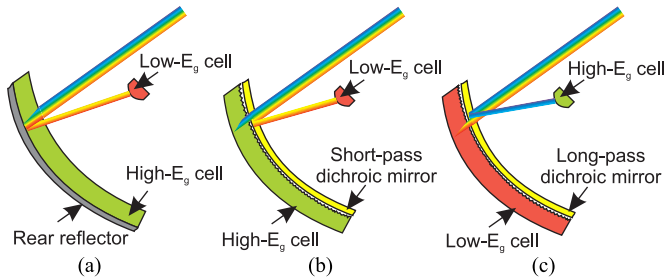

Fig. 1. Three PVMirror trough configurations illustrating the range of possible embodiments. (a) Smooth, wide-bandgap cell and specular reflector, (b) textured wide-bandgap cell and short-pass dichroic mirror, and (c) textured narrow-bandgap cell and long-pass dichroic mirror. Note that the supporting structures that determine the PVMirror geometry (e.g., curved glass on which the PV cells are affixed) are not shown in this conceptual schematic.

first (Fig. 1(a)) uses a smooth (i.e., lacking surface texture that would scatter light) wide-bandgap PV cell with a rear mirror. The PV cell absorbs all super-bandgap light while specularly reflecting all sub-bandgap light to a common focus, where a narrow-bandgap cell or other receiver sits that is intended to use the concentrated light. The second embodiment, shown in Fig. 1(b), uses the same wide-bandgap PV cell but with a textured rather than smooth surface. In this case, it is necessary to add a spectrally selective dichroic mirror in front of the cell, which transmits only super-bandgap light while concentrating sub-bandgap light at the focus. The advantage of this design (and the next) is that, for indirect-bandgap cells, the textured surface better traps the near-bandgap light transmitted through the coating. (In a slight modification, the dichroic mirror can be a band-pass design that transmits only near-bandgap light so that both sub-bandgap and very-high-energy photons—which lose most of their energy to thermalization if absorbed in the PV cell—are rejected to the focus. This is appropriate if the converter at the focus is wavelength agnostic—i.e., not another PV cell as in Fig. 1(b).) The third embodiment represented in Fig. 1(c) is similar to the second, but switches the PV cell positions so that narrow-bandgap cells (e.g., silicon cells) form the PVMirror and a wide-bandgap cell is positioned at the focus. With an adjusted (long-pass) dichroic mirror, all high-energy photons are reflected to the focus while low-energy photons are absorbed in the PVMirror. In this unusual tandem configuration, sunlight hits the "bottom" cell first rather than the "top" cell. As the per-square-meter cost of silicon PV cells is lower than any comparable-efficiency wide-bandgap PV cell, this configuration can be more quickly adopted by the market.

Manufacturing of PVMirrors should require little, if any, new process and equipment development. For thin-film PV cells, PVMirrors can be made by depositing the cells either on curved glass or on flat glass segments that are then arranged to approximate the desired curvature. In the trough configuration, the latter would look like SunPower or Cogenra's low-concentration silicon PV technology, but with wide-bandgap PVMirrors in the place of silvered mirrors, as illustrated in Fig. 2. Alternatively, thin-film cells can be deposited on a flexible metal sheet that is then mounted curved, or on plastic or metal foil that is then laminated to a curved surface. For wafer-based cells, lamination

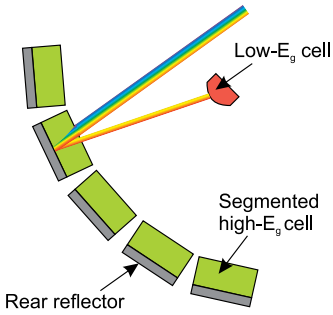

Fig. 2. The PVMirror configuration of Fig. 1(a) but with a segmented trough consisting of flat PVMirror strips.

to either curved glass or flat segments is likely the best option. In fact, one can think of a PVMirror as simply a curved (or segmented) PV module with a sophisticated anti-reflection coating (Fig. 1(b) and (c)) or an excellent specular rear reflector (Fig. 1(a)). In the Fig. 1(b) and (c) configurations, commercial cells (thin film or wafer based) with any texture can be used, whereas for the Fig. 1(a) configuration, smooth (and parallel) cell surfaces are required to successfully direct reflected light to the focus. In this case, either conformal layers (for thin-film cells) or polished wafers are needed. This does not necessarily imply expensive chemical–mechanical polishing that yields atomically flat surfaces; for example, for silicon PV cells, our recent results indicate that inexpensive HF/HNO_3 acid-based chemical polishing yields >99% specularity of reflected light [25], [26]. If a dichroic mirror is to be used, it can be sputtered or evaporated onto the inner side of the front glass or plastic sheet, or a polymer optical film like those from 3M can be applied on the inner or outer side of the glass or plastic [27].

An advantage of PVMirrors for PV–PV tandems is that—like for all optically coupled tandems—the choice of top and bottom cells is free of lattice- and current-matching restrictions. Furthermore, either the wide- or narrow-bandgap cell can be placed under concentration at the focus depending on the relative cell costs. Alternatively, a non-PV solar converter can receive the concentrated light, making PVMirrors amenable to hybridization with technologies that offer additional functionality, such as storage with solar thermal systems. An additional advantage is that the PVMirror itself has a lower one-sun operating temperature than a comparable flat-plate PV module as it reflects sub-bandgap light (Fig. 1(a) and (b)), super-bandgap light (Fig. 1(c)), or both if using a band-pass dichroic mirror. This reduces infrared parasitic absorption or thermalization of electron–hole pairs generated by high-energy photons, both of which increase the operating temperature of a PV module above the ambient temperature.

However, the greatest benefit of PVMirrors over most other tandem concepts—and concentrating solar thermal power (CSP) systems, incidentally—is that PVMirrors make use of a portion of the diffuse light, whereas concentrator systems cannot. This is enabled by the unusual PVMirror design in which the sub-cell that forms the PVMirror receives one-sun, global irradiation, while the sub-cell at its focus receives concentrated direct light. Fig. 3 shows that, under standard (cloud-free) AM1.5 conditions, diffuse light still accounts for 10% of the global incident power. Furthermore, Rayleigh scattering blue-shifts the spectrum so that about 80% of the diffuse power is at wavelengths below 800 nm; this means that even a relatively wide-bandgap cell can capture most of the blue-sky diffuse light. Fig. 4 shows the global solar insolation and relative diffuse percentage for various geographic locations in the USA; the most striking feature is that there is much more diffuse light than the 10% attributable to atmospheric scattering under AM1.5 conditions. The additional diffuse light is primarily due to cloud scattering, and from data measured by NREL, we know the associated spectrum to be relatively white, much like the AM1.5 direct or global spectra [28].

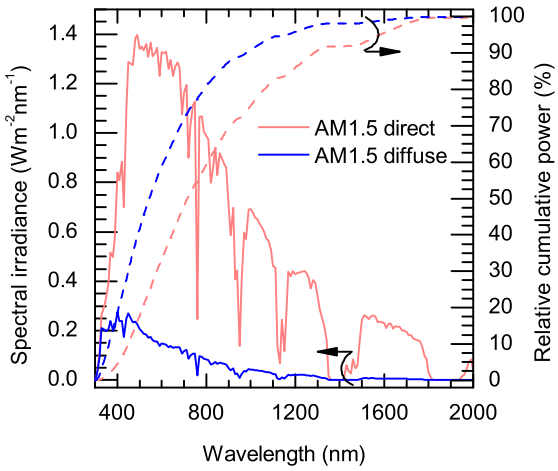

Fig. 3. AM1.5 direct spectrum and AM1.5 diffuse spectrum, calculated as the difference between the AM1.5 global (not shown) and AM1.5 direct spectra. Also shown is the relative cumulative power (fraction of power below a given wavelength) for the AM1.5 direct and AM1.5 diffuse spectra.

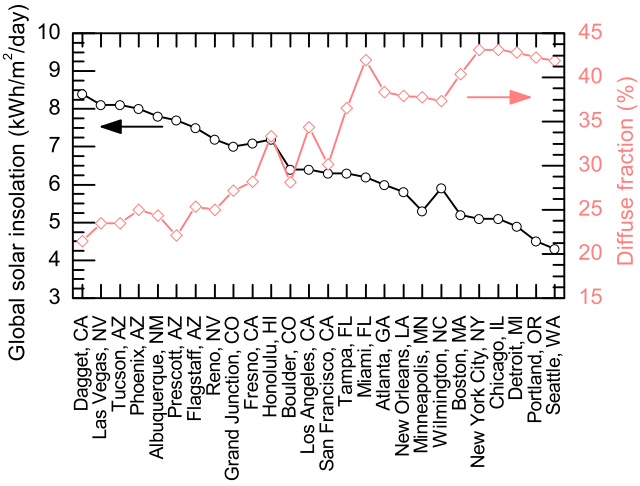

Fig. 4. Global insolation and fraction of diffuse radiation on a North-South-axis tracking plate for different locations in the U.S. [16].

III. Case Study I: PV–PV Tandem

We believe that future high-efficiency tandems for one-sun or low-concentration applications will likely be based on silicon, as silicon PV already has GW-scale production capacity and

has proved itself to be a difficult technology to displace in the past [29]. More importantly, the bandgap of silicon is close to ideal for a bottom cell in tandems. The challenge is to find a top cell with the right bandgap and high enough efficiency to produce a tandem that outperforms the (already excellent) silicon cell on its own. A GaInP cell has been demonstrated that would be suitable: the absorber had a bandgap of 1.8 eV and the cell had a record efficiency of 20.8% [30]. Unfortunately, a 4% lattice mismatch limits its application on silicon in the conventional two-terminal monolithically integrated tandem configuration. Wafer-bonding is one route to escape epitaxy, and Derendorf *et al.* demonstrated a 20.5%-efficient wafer-bonded multi-junction cell under one-sun illumination [31]. An alternative is to grow epitaxial top cells of other, near-lattice-matched III–V materials such as GaAsP; Connolly *et al.* predicted a GaAsP/Si tandem cell with an efficiency of 32.2% [32]. With the emergence of low-cost halide perovskite PV cells with rapidly improving efficiencies, perovskite/Si tandems have also become a popular research topic. A theoretical analysis by Loper *et al.* showed that a 35%-efficient tandem is attainable, but will require proper material and device development [33]. Another promising candidate to pair with silicon is CdTe-based II–VI materials, which Garland *et al.* calculated may result in higher multi-junction cell efficiencies (and with lower cost) than is possible with III–V multi-junction cells [34]. Besides silicon, CdTe is the only competitive technology in the present flat-plate PV market, and ternary alloys of CdTe with Mg, Zn, or Mn have bandgaps that vary from 1.48 eV to 3.5 eV [35], thus spanning the 1.6–1.8 eV range that is required for current matching with silicon [36]. Xu *et al.* calculated that, using $Cd_{0.5}Zn_{0.5}Te$ with a bandgap of 1.8 eV as a top cell on silicon, a one-sun efficiency of 35.4% is possible [37].

To investigate the potential of PVMirrors for silicon-based tandems, we consider an example in which a hypothetical CdMgTe PV cell with a 1.8 eV bandgap and an efficiency of 21.1% (under one-sun AM1.5 global illumination) is paired with a 22%-efficient silicon heterojunction cell. The external quantum efficiency (EQE) and other key one-sun parameters of each cell separately (prior to tandem formation) are shown in Fig. 5. The short-circuit current density (J_{SC}) values were calculated by integrating the product of the EQE and AM1.5 global spectral photon flux. The EQE of the silicon heterojunction cell was measured, whereas the EQE of the hypothetical CdMgTe cell was obtained by shifting the EQE of a record CdTe cell [38]. The resulting J_{SC} of 20.37 mA/cm^2 agrees with that modeled by Xu *et al.* [37] The open-circuit voltage (V_{OC}) of the silicon heterojunction cell was assumed to be 730 mV—below what we regularly measure for cells made in our lab—and the V_{OC} of the hypothetical CdMgTe cell was set to 1.31 V, consistent with that demonstrated by Carmody *et al.* [39]. A conservative fill factor *(FF)* of 79% was taken for both cells—Panasonic has demonstrated 83.2% in a silicon heterojunction cell and First Solar reported 80.0% in a CdTe cell [40]. The "spectral efficiency" shown in Fig. 5(b) was calculated according to:

$$\text{Efficiency}(\lambda) = J_{SC}(\lambda) \cdot V_{OC} \cdot FF, \tag{1}$$

Cell	η (%)	E_g (eV)	V_{OC} (V)	J_{SC} (mA/cm^2)	FF (%)
CdMgTe	21.1	1.8	1.31	20.37	79.0
Silicon	22.4	1.1	0.73	38.74 (20.84)	79.0

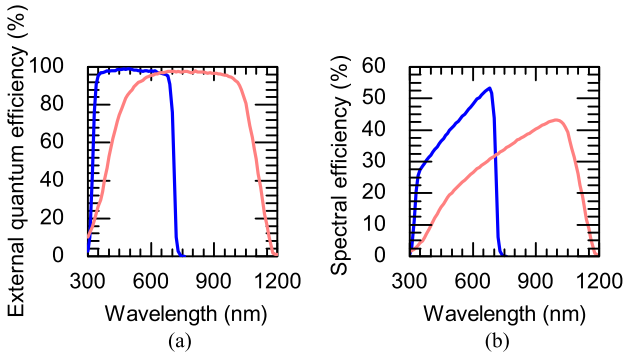

Fig. 5. Performance of the CdMgTe and silicon heterojunction PV cells used in the tandem simulations. The reported values are those that would be measured for the individual cells with (normally incident) AM1.5 global illumination. The J_{SC} value in parentheses is the calculated current density for the silicon heterojunction cell when used as the bottom cell in a (one-sun) monolithic tandem. (a) EQE and (b) photon-to-DC-power spectral efficiency of the CdMgTe (blue) and silicon heterojunction (red) PV cells.

where

$$J_{SC}(\lambda) = q\frac{\lambda}{hc}\text{EQE}(\lambda) \cdot F(\lambda), \tag{2}$$

and q, h, and c have their usual meanings, λ is the wavelength in nm, and F is the spectral irradiance of the AM1.5 global spectrum in $\text{W}\cdot\text{m}^{-2}\cdot\text{nm}^{-1}$. This spectral efficiency plot is helpful in predicting the maximum possible tandem device performance when coupling two cells because the output of the cells can be compared directly at any desired wavelength.

To assemble the two sub-cells into a tandem, the CdMgTe top cell is arranged into a segmented parabolic shape to form a PVMirror (Fig. 2) and the silicon heterojunction bottom cell is placed at the (line) focus. We simulated the performance of this PVMirror tandem system assuming 20X geometric concentration at the focus, and compared the result with that of a monolithic tandem (employing the same sub-cells) under both one-sun illumination and 20X geometric concentration. First, we calculated the efficiencies that would be measured in a laboratory setting with a flash tester that illuminates the cells with the AM1.5 global spectrum at nominally normal angle of incidence (no diffuse light). (This procedure is a compromise between those used to certify the efficiencies of flat-plate and concentrated PV cells.) To do this, the J_{SC} of each sub-cell was calculated from its EQE (Fig. 5) and the specific spectrum and irradiance it receives (e.g., the bottom cell is illuminated only with light not absorbed in the top cell and is under concentration in two of the configurations). Next, the one-sun current–voltage parameters in Fig. 5 were used to calculate the V_{OC} and *FF* of each sub-cell given the photogeneration just calculated. Finally, the power outputs of the sub-cells were summed and normalized to the incident power. We assumed no efficiency loss in any of the cells during tandem formation, i.e., no optical losses for the PVMirror or 20X monolithic tandems, and no current- or lattice-matching losses in either monolithic tandem. The in-lab

TABLE I
COMPARISON OF CDMGTE/SI MONOLITHIC AND PVMIRROR TANDEMS

	20X PVMirror tandem	One-sun monolithic tandem	20X monolithic tandem
Current matching	Not required	Required	Required
Lattice matching	Not required	Required	Required
Diffuse light collection	300–700 nm	300–1200 nm	None
Material consumption	Full-area CdMgTe, 1/20-area Si	Full-area CdMgTe and Si	1/20-area CdMgTe and Si
In-lab efficiency (AM1.5G, normal)	34.3%	33.4%	35.6%
Solar resource (Phoenix)	Direct light: 6 kWh/m^2/day	Diffuse light: 2 kWh/m^2/day	
Outdoor efficiency	32.5%	33.4%	26.5%
DC energy output	2.60 kWh/m^2/day	2.67 kWh/m^2/day	2.12 kWh/m^2/day
Solar resource (Miami)	Direct light: 3.6 kWh/m^2/day	Diffuse light: 2.8 kWh/m^2/day	
Outdoor efficiency	28.8%	32.4%	20.5%
DC energy output	1.84 kWh/m^2/day	2.07 kWh/m^2/day	1.31 kWh/m^2/day

efficiencies, therefore, reflect the maximum attainable values given the sub-cells and the chosen tandem configurations.

To compare the tandem configurations in realistic outdoor settings, we also calculated their outdoor efficiencies and annually averaged daily energy outputs when placed on North–South-axis trackers in Phoenix and Miami, which have diffuse light fractions of 25% and 42%, respectively. Direct and diffuse light were treated separately and—in Phoenix—were assumed to have the AM1.5 direct and AM1.5 diffuse (global minus direct) spectra shown in Fig. 3, normalized to Phoenix's direct and diffuse fractions. Calculations for Miami were the same except the AM1.5 global spectrum was used in place of the AM1.5 diffuse spectrum (for the 42% diffuse fraction). This variation in the assumed spectrum for diffuse light represents our best attempt to approximate the local conditions: most days in Phoenix are cloud-free, and thus, the diffuse light there should be blue-shifted[1]; many days in Miami are cloudy, and we expect cloud scattering to result in a comparatively white spectrum. Independent of location, our calculations assumed that the one-sun monolithic tandem absorbs both direct and diffuse light, the 20X monolithic tandem absorbs only the direct light, and the 20X PVMirror tandem absorbs both in the CdMgTe top cell but only direct light in the silicon heterojunction bottom cell.[2] We did not account for degradation in V_{OC} due to the increased operating temperature of the cells in outdoor environments. The power output of each tandem was normalized to the global input power to arrive at the outdoor efficiency, and the efficiency was multiplied by the annually averaged daily global insolation on a North–South-axis tracker (given in Table I) to determine the energy output. Table I displays the results of these calculations, as well as the in-lab efficiencies discussed above and the advantages and drawbacks of each configuration.

The 20X monolithic tandem has the highest in-lab efficiency, but has the lowest outdoor energy output as it captures no diffuse light. This discrepancy becomes larger for locations with a higher fraction of diffuse light: For example, in Miami, the 20X monolithic tandem's average efficiency is only slightly more than half the cell's in-lab efficiency. The 20X PVMirror tandem has a higher in-lab efficiency than the one-sun monolithic tandem because the silicon heterojunction bottom cell is under concentration, but a lower in-lab efficiency than the 20X monolithic tandem, for which both cells are under concentration. More importantly, the PVMirror tandem has a significantly higher outdoor energy output than the 20X monolithic tandem and an output nearly as high as the one-sun monolithic tandem because it both collects most of the available diffuse light in the CdMgTe top cell, especially in blue-sky Phoenix, and it benefits from the aforementioned concentration in the bottom cell. Although the PVMirror tandem energy output is slightly lower than that of the (current-matched) monolithic tandem, the levelized cost of electricity generated by the PVMirror tandem would be lower (given the same balance-of-systems cost) because it consumes 20 times fewer silicon cells.

The above analysis considered ideal tandems in which two individual sub-cells were coupled without loss. Real PVMirror tandems are expected to approach much closer to this ideal than monolithic tandems. In PVMirror tandems, the sub-cells are fabricated separately and on their own respective substrates (if used), which allows for complete freedom in optimization of each sub-cell; the dominant challenges in monolithic tandems—material and process compatibility—are eliminated. Consequently, PVMirror tandems should be free of, e.g., high recombination currents at defects induced during epitaxy and parasitic absorption in graded buffer layers—common problems in monolithic tandems. In addition, monolithic tandems will frequently experience current mismatch in real meteorological conditions even when designed to be current matched in the lab [41], [42], resulting in power losses not incurred by PVMirror tandems and other four-terminal designs. The largest anticipated losses in real PVMirror tandems are an elevated temperature of the silicon cell under concentration (which is mitigated by sending it only infrared light), scattering of reflected light due to PVMirror soiling, an inhomogeneous distribution of concentrated light on the silicon cell, and parasitic absorption of sub-bandgap light in the CdMgTe top cell, which will reduce the illumination on the bottom cell. Most sub-bandgap absorption is due to free-carrier absorption (e.g., in doped layers, transparent conductive oxides, or metals) and must be carefully controlled

[1]Assuming the AM1.5 global spectrum instead in Phoenix (cloud scattering dominates Rayleigh scattering) changes the results by less than 5% relative.

[2]Note that, although the geometric concentration ratio is 20, the effective concentration ratio (generation rate multiplier) in the bottom cell is approximately 8 in Phoenix and 6 in Miami because only direct light not absorbed in the top cell reaches the PVMirror focus.

TABLE II
CSP PERFORMANCE USED IN CASE STUDY II CALCULATIONS

Tracking and trough absorption loss	Receiver optical loss	Receiver thermal loss	Rankine efficiency	Power block parasitic loss	Thermal loss for stored heat	CSP efficiency*
19%	12%	20%	35%	10%	9%	18.0%

*Average system efficiency with respect to direct light only and with no thermal storage.

for PVMirror configurations that use absorptive filtering (as in Figs. 1(a) and 2).

Are PVMirror tandems dependent upon the prior development of cheap, efficient, wide-bandgap, thin-film, one-sun top cells like CdMgTe? No. As shown in Fig. 1(c), it is possible to move the wide-bandgap top cell to the focus and use a narrow-bandgap cell with an additional long- or band-pass dichroic mirror to form the PVMirror. This configuration is economically preferred if the top cell is more expensive than the bottom cell, as the cost of the cell at the focus is always discounted by the concentration ratio. An example is a PVMirror with silicon cells directing short wavelengths to a small-area, high-efficiency (and expensive) GaInP cell.

IV. CASE STUDY II: PV–CSP TANDEM

PVMirrors can also be used with non-PV solar energy converters designed to operate under concentration, including, e.g., CSP receivers. There are four main types of CSP collectors—trough, dish, Fresnel mirror, and heliostat—and PVMirrors can in principle be used in place of any of them by adopting the right curvature. Generally, all three PVMirror configurations introduced in Fig. 1 suit all four types of collectors; however, heliostats are unique in that they direct light to a fixed central receiver, which means that there is a large variation in the angle of incidence on each heliostat throughout the day. As dichroic mirrors like those in Fig. 1(b) and (c) tend to be sensitive to angle of incidence, particularly at grazing angles, the specular-rear-reflector PVMirror configuration shown in Fig. 1(a) is preferred for heliostats.

In this case study, we consider utility-scale trough CSP, which employs a mirrored parabolic trough on a North–South-axis tracker to reflect all wavelengths to a black receiver tube (average concentration on the tube of approximately 27X) filled with a flowing heat-transfer fluid. Trough CSP is the most mature of the CSP technologies but has a low demonstrated average efficiency of 10–15% (with respect to the global insolation) [43]. There are two reasons for this modest efficiency: no diffuse light is intercepted by the receiver tube and the conversion of direct light to electrical power suffers from the many small losses given in Table II [44]. These are compounded to yield an efficiency of 18.0% with respect to direct light only. By replacing mirrored troughs with PVMirrors, we expect to mitigate both CSP losses: The PV cells will collect diffuse (in addition to direct) light within a particular spectral band, and this light will be converted to electrical power with efficiencies much greater than 18.0%. It is tempting to simply replace the CSP troughs with flat-plate PV modules—SunPower modules on single-axis trackers would yield efficiencies of approximately 21% with respect to the global insolation—but CSP offers the advantage of

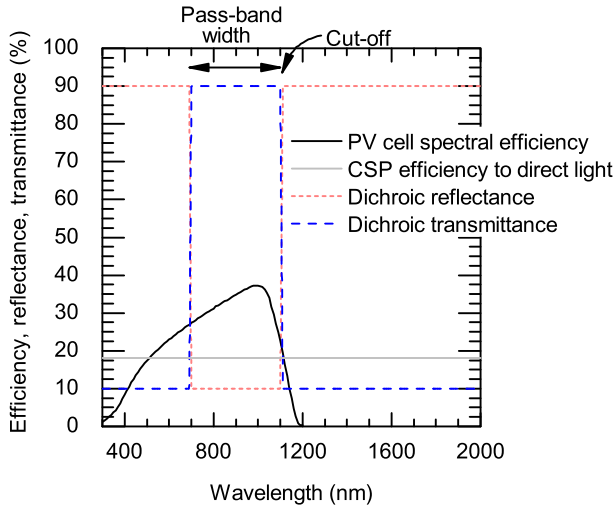

Fig. 6. Photon-to-AC-power spectral efficiencies of the silicon heterojunction PVMirror and trough CSP system used in calculations for Case Study II. Also shown are the assumed reflectance and transmittance of the band-pass dichroic mirror located in front of the PV cell.

economical energy storage and thus dispatchable electricity, as well as superior efficiency at long and short wavelengths, which are poorly used by PV cells. A PV–CSP tandem utilizing PVMirrors is expected to match the efficiency of flat-plate PV while retaining the same total dispatchable-electricity capacity of CSP.

We assumed a trough PVMirror with the same silicon heterojunction PV cells that were used in Case Study I, but with the cells on the glass trough to form the PVMirror rather than at its focus. Fig. 6 again shows the spectral efficiency of this cell—this time including additional losses described below—as well as the wavelength-agnostic CSP efficiency (to direct light only). Note that wavelengths shorter than 500 nm or longer than 1100 nm are best reflected to the receiver tube, as CSP has a higher conversion efficiency than the silicon heterojunction cell at these wavelengths. We thus included a band-pass dichroic mirror in the PVMirror to arrive at a configuration similar to those depicted in Fig. 1(b) and (c). The band-pass mirror was assumed to have 90% transmittance in the pass-band and 90% reflectance in the reject bands (shown in Fig. 6), and the pass-band width and cut-off wavelength (transition from transmitting to reflecting) were varied. Note that polymer dichroic mirrors with better than the assumed 90%/90% performance are available from, e.g., 3M for $\sim$20 \$/m^2. The PVMirror PV–CSP tandem efficiency and energy output was modeled in Phoenix and Miami with the same methodology used in Case Study I, but additional PV losses were included to ensure that PV and CSP were equitably compared. In particular, this case study assumed a 10% cell-to-module or cell-to-PVMirror loss and a 4% DC-to-AC

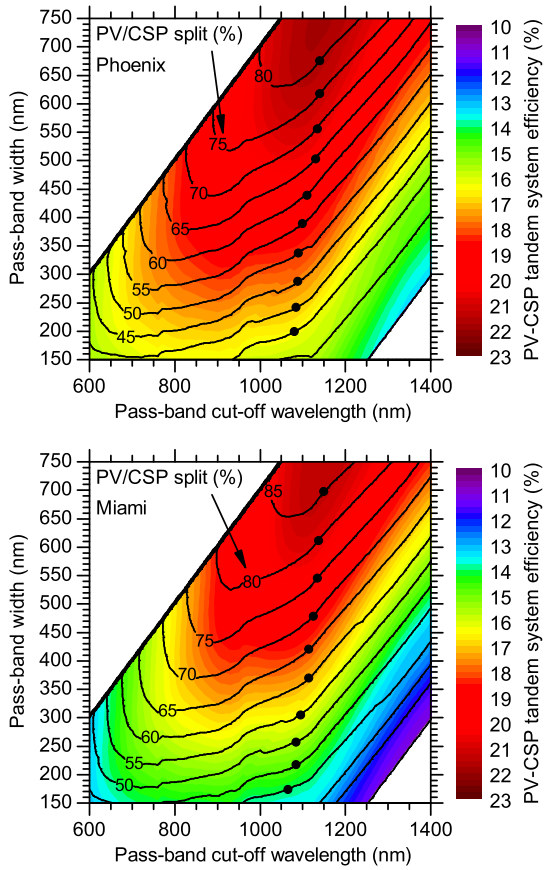

Fig. 7. Performance of a PV–CSP tandem located in Phoenix or Miami as a function of the pass-band width and cut-off wavelength of the band-pass dichroic mirror. The color contours represent the outdoor system efficiency (with respect to the global insolation) assuming no thermal storage, and the line contours represent the PV/CSP power output split in percentage of PV. The black dots indicate the band-pass mirror characteristics that result in the highest efficiency for a given PV/CSP split.

inverter loss (all tandems in Case Study I generate DC power and were compared on the cell level for simplicity; thus, these losses were neglected). We assumed that the PV–CSP tandem operates with the same Rankine efficiency of a pure CSP system (given in Table II), which requires that the heat-transfer fluid reach the same outlet temperature despite reduced heat flux (i.e., by a reduced fluid flow).

The first step in modeling the PV–CSP tandem is to determine the optimal band-pass dichroic mirror characteristics for the PVMirror. Fig. 7 displays color contour plots of the outdoor efficiency of PV–CSP tandems in Phoenix and Miami for a range of mirror pass-band widths and cut-off wavelengths. Also shown with line contours is the PV/CSP split—the fraction of the AC power output that comes from the PV cells. Fig. 7 assumes no dispatchable electricity; thermal storage is treated separately below. The highest efficiency of approximately 21.8% can be achieved in Phoenix with a wide pass-band that sends most of the sunlight to the PV cells (as expected from Fig. 6). However, this has the consequence that a small fraction of light is sent to the receiver tube, resulting in CSP contributing only 20% of the total output power. It is unlikely that the cost of a CSP system, with the associated thermal energy storage, power block, and collector field, would be justified for this small power output. Although a unique feature of this tandem is that the PV/CSP split can be varied according to the desired plant design, a 50% split is likely a sensible balance between higher efficiency and greater storage capacity. To achieve the highest efficiency with this constraint, Fig. 7 indicates that the pass-band should be 260–340 nm wide, depending on the diffuse fraction, and have a cut-off wavelength of roughly 1100 nm, independent of diffuse fraction (and, in fact, independent of the prescribed PV/CSP split).

Table III compares the outdoor efficiencies and annually averaged daily energy outputs for a PV–CSP tandem with a 50% split (assuming the optimum mirrors identified by the black dots on the 50% lines in Fig. 7), a flat-plate PV system with the same heterojunction cells on the same North–South-axis tracker, and a trough CSP system. The PV and CSP systems are conceptually like PV–CSP tandems with splits of 100% and 0%, respectively, corresponding to either omitting the dichroic mirror or making it a broadband reflector. As in Fig. 7, Table III assumes no dispatchable electricity. The PV–CSP tandem using a PVMirror generates nearly as much electricity in Phoenix as the pure PV system and 36% more than the pure CSP system; in Miami it falls short of the PV system[3] but still produces almost as much energy as the pure CSP system in Phoenix. Consequently, PVMirrors may extend the geographical reach of CSP, which has traditionally been limited to the high-direct-insolation Southwest.

At first glance, Table III appears to indicate that a PV–CSP tandem with a 50% split is inferior to a pure PV system in all locations; however, Table III ignores the thermal storage capacity of both the PV–CSP tandem and the pure CSP system. With increasing PV penetration, the marginal value of additional PV on the electricity grid is expected to diminish [45] and utilities that want to install renewable power plants will begin adding battery storage or return to CSP with thermal storage. Given a 9% loss in energy of stored heat, the outdoor system efficiency is shown in Fig. 8 as a function of CSP storage fraction for PV–CSP tandems, a pure CSP system, and a pure PV system. The efficiencies for a storage fraction of zero correspond to those in Table III. On average, storing all of the heat generated in the receiver tube prior to electricity generation (all CSP electricity is dispatchable) results in a 1% absolute decrement in system efficiency. For a typical pure CSP system, roughly one-third of its electricity (0.36 kWh/m^2/day in Phoenix) is dispatchable (e.g., Solana operates for roughly twelve hours a day and is designed for six hours of storage), and it will operate at 13.2% efficiency in Phoenix according to Fig. 8. For a PV–CSP tandem, the dispatchable electricity is the product of the PV/CSP split, CSP storage fraction, and total system energy output. Thus, PV–CSP tandems in Phoenix with a 40% split and 46% storage fraction, 50% split and 51% storage fraction, and 70% split and 74% storage fraction will all have 0.36 kWh/m^2/day of dispatchable electricity as well, but will operate with efficiencies of 16.4, 17.7, and 20.2%, respectively (see dots in Fig. 8). With a properly selected band-pass dichroic mirror, a PVMirror-based PV–CSP tandem can therefore operate—in principle—at higher

[3]The efficiency of the PV system is higher in Miami than in Phoenix because the diffuse light in Phoenix was assumed to be bluer and thus poorly matched to silicon's bandgap. Also the angular dependence of reflection from the front surface of the module was not considered, so the higher diffuse fraction in Miami comes with no penalty.

TABLE III
COMPARISON OF A PV–CSP TANDEM WITH TROUGH CSP AND PV SYSTEMS

	PV–CSP tandem system (50% split)	Trough CSP system	PV system
Solar resource (Phoenix)	Direct light: 6 kWh/m^2/day	Diffuse light: 2 kWh/m^2/day	
Outdoor efficiency	18.3%	13.5%	19.0%
AC energy output	1.46 kWh/m^2/day	1.08 kWh/m^2/day	1.52 kWh/m^2/day
Solar resource (Miami)	Direct light: 3.6 kWh/m^2/day	Diffuse light: 2.8 kWh/m^2/day	
Outdoor efficiency	15.5%	10.5%	19.4%
AC energy output	0.99 kWh/m^2/day	0.67 kWh/m^2/day	1.24 kWh/m^2/day

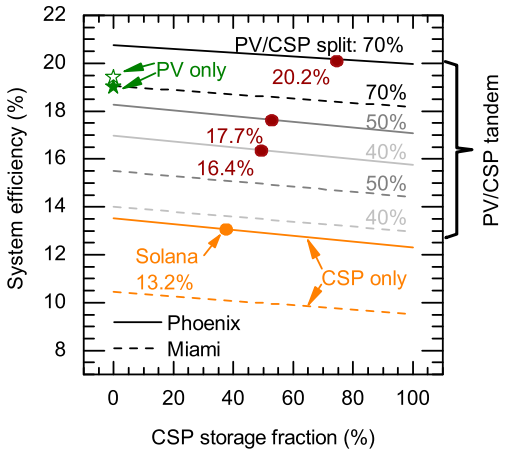

Fig. 8. Outdoor system efficiency (with respect to the global insolation) of a PV–CSP tandem as a function of the fraction of the CSP AC power output that is dispatchable. Stored heat is assumed to incur a 9% loss. Data are shown for PV/CSP splits of 40–70%, and the product of the PV/CSP split and CSP storage fraction is the fraction of the total system AC power output that is dispatchable. Also plotted are the efficiencies of pure CSP and PV systems. The dots and adjacent system efficiencies correspond to configurations that provide 0.36 kWh/m^2/day of dispatchable electricity.

efficiency than a pure PV system while maintaining the full dispatchability of a pure CSP system. In practice, and as discussed previously, it is likely preferable to operate with a more equitable PV/CSP split and even higher storage capacity to justify the cost of the power block and thermal energy storage.

V. OUTLOOK

The universality of the PVMirror design lies in its ability to turn a narrow- or wide-bandgap PV cell into a tandem with nearly any other solar energy converter. We analyzed two case studies that demonstrate the great flexibility of PVMirrors: In one, a wide-bandgap PV cell was coupled to a second PV cell via absorptive filtering; in the other, a narrow-bandgap PV cell was coupled to a thermal absorber via reflective filtering. In both cases, the PVMirror tandems performed well compared to existing technologies. Other hybridizations can also be envisioned; the key is to find converters that "like" input spectra complementary to the spectrum absorbed by the cells in the PVMirror. For example, in solar chemistry, high-energy photons are required to degrade hazardous organic chemical compounds [46]. A possible detoxification process could thus be to flow hazardous chemicals through a pipe located at the focus of a PVMirror employing narrow-bandgap cells and a dichroic mirror. This would particularly make sense if electricity were also required in the detoxification process (or by the plant facilities), since it would be generated on site [47].

This paper has focused on efficiency and energy output, but the astute reader will also want to know about cost. A good "sanity check" is to compare the installed cost per annual energy yield (equivalent to levelized cost of electricity given similar depreciation times and operating costs) of a PVMirror system and each of its coupled solar energy converters individually. For example, comparing the PV–CSP tandem and pure CSP systems in Case Study II, the tandem saves the cost of the silver on the mirrors but adds the cost of PV cells, a band-pass dichroic mirror, lamination materials, inverters, and field wiring. We estimate that this corresponds to a 30% increase in the cost of the collector field, which itself comprises one-third the cost of a trough CSP power plant [44], leading to a 10% increase in the total installed system cost. For a total dispatchable electricity (or storage) capacity identical to a pure CSP system, we calculated that the tandem has up to a 53% greater annual energy yield, corresponding to a 28% savings in cost per energy. Comparing the PV–CSP tandem and pure PV system in Case Study II, the tandem adds the cost of glass curving and the associated additional support, receiver tubes and fluid, a power block, and thermal energy storage. We estimate that this doubles or triples the installed cost, depending on the size of the power block, for no significant increase in energy output. Consequently, a PV–CSP tandem is preferred over a PV system only if the utility company values dispatchable electricity at a substantial premium over variable electricity. This may seem unlikely, but the calculation is even less favorable when comparing pure CSP and pure PV, yet CSP power plants exist. In general, a PVMirror-based tandem is economically competitive when the two constituent solar energy converters have significant overlap in their most expensive components or infrastructure (e.g., glass, trackers, land); in this case, the marriage of the converters eliminates duplication of the associated costs.

REFERENCES

[1] D. M. Powell, M. T. Winkler, H. J. Choi, C. B. Simmons, D. B. Needleman, and T. Buonassisi, "Crystalline silicon photovoltaics: A cost analysis framework for determining technology pathways to reach baseload electricity costs," *Energy Environ. Sci.*, vol. 5, pp. 5874–5883, Mar. 2012.

[2] A. Goodrich, P. Hacke, Q. Wang, B. Sopori, R. Margolis, T. L. James, and M. Woodhouse, "A wafer-based monocrystalline silicon photovoltaics road map: Utilizing known technology improvement opportunities for further reductions in manufacturing costs," *Sol. Energy Mater. Sol. Cells*, vol. 114, pp. 110–135, Jul. 2013.

[3] M. A. Green, K. Emery, Y. Hishikawa, W. Warta, and E. D. Dunlop, "Solar cell efficiency tables (version 44)," *Progr. Photovoltaics*, vol. 22, pp. 701–710, Jul. 2014.

[4] D. D. Smith, P. Cousins, S. Westerberg, R. De Jesus-Tabajonda, G. Aniero, and Y. C. Shen, "Toward the practical limits of silicon solar cells," *IEEE J. Photovoltaics*, vol. 4, no. 6, pp. 1465–1469, Nov. 2014.

[5] A. Richter, M. Hermle, and S. W. Glunz, "Reassessment of the limiting efficiency for crystalline silicon solar cells," *IEEE J. Photovoltaics*, vol. 3, no. 4, pp. 1184–1191, Oct. 2013.

[6] M. A. Green, K. Emery, Y. Hishikawa, W. Warta, and E. D. Dunlop, "Solar cell efficiency tables (version 40)," *Prog. Photovoltaics*, vol. 20, pp. 606–614, Aug. 2012.

[7] W. Shockley and H. J. Queisser, "Detailed balance limit of efficiency of P-N junction solar cells," *J. Appl. Phys.*, vol. 32, p. 510, 1961.

[8] M. A. Green, "Limiting photovoltaic efficiency under new ASTM International G173-based reference spectra," *Prog. Photovoltaics*, vol. 20, pp. 954–959, Dec. 2012.

[9] M. A. Green, "Third generation photovoltaics: Solar cells for 2020 and beyond," *Phys. E-Low-Dimensional Syst. Nanostructures*, vol. 14, pp. 65–70, Apr. 2002.

[10] P. Würfel, *Physics of Solar Cells: From Basic Principles to Advanced Concepts*. New York, NY, USA: WILEY-VCH, 2009.

[11] C. H. Henry, "Limiting efficiencies of ideal single and multiple energy-gap terrestrial solar-cells," *J. Appl. Phys.*, vol. 51, pp. 4494–4500, 1980.

[12] R. R. King, D. C. Law, K. M. Edmondson, C. M. Fetzer, G. S. Kinsey, H. Yoon, R. A. Sherif, and N. H. Karam, "40% efficient metamorphic GaInP/GaInAs/Ge multi-junction solar cells," *Appl. Phys. Lett.*, vol. 90, p. 183516, Apr. 30, 2007.

[13] W. Guter, J. Schone, S. P. Philipps, M. Steiner, G. Siefer, A. Wekkeli, E. Welser, E. Oliva, A. W. Bett, and F. Dimroth, "Current-matched triple-junction solar cell reaching 41.1% conversion efficiency under concentrated sunlight," *Appl. Phys. Lett.*, vol. 94, p. 223504, Jun. 1, 2009.

[14] F. Dimroth, M. Grave, P. Beutel, U. Fiedeler, C. Karcher, T. N. D. Tibbits, E. Oliva, G. Siefer, M. Schachtner, A. Wekkeli, A. W. Bett, R. Krause, M. Piccin, N. Blanc, C. Drazek, E. Guiot, B. Ghyselen, T. Salvetat, A. Tauzin, T. Signamarcheix, A. Dobrich, T. Hannappel, and K. Schwarzburg, "Wafer bonded four-junction GaInP/GaAs//GaInAsP/GaInAs concentrator solar cells with 44.7% efficiency," *Prog. Photovoltaics*, vol. 22, pp. 277–282, Mar. 2014.

[15] S. Corporation. (2012). *Sharp Develops Concentrator Solar Cell with World's Highest Conversion Efficiency of 43.5%*. [Online]. Available: http://sharp-world.com/corporate/news/120531.html

[16] W. Marion and S. Wilcox. (1994). "Solar radiation data manual for flat-plate and concentrating collectors," [Online]. Available: http://rredc.nrel.gov/solar/pubs/redbook/

[17] A. V. Shah, H. Schade, M. Vanecek, J. Meier, E. Vallat-Sauvain, N. Wyrsch, U. Kroll, C. Droz, and J. Bailat, "Thin-film silicon solar cell technology," *Prog. Photovoltaics*, vol. 12, pp. 113–142, Mar.–May 2004.

[18] A. G. Imenes and D. R. Mills, "Spectral beam splitting technology for increased conversion efficiency in solar concentrating systems: A review," *Sol. Energy Mater. Sol. Cells*, vol. 84, pp. 19–69, Oct. 2004.

[19] R. L. Moon, L. W. James, H. A. Vanderplas, R. O. Yep, G. A. Antypas, and Y. Chai, "Multigap solar cell requirements and the performance of AlGaAs and Si cells in concentrated sunlight," presented at the 13th Photovoltaic Spec. Conf., Washington, DC, USA, 1978.

[20] B. Mitchell, G. Peharz, G. Siefer, M. Peters, T. Gandy, J. C. Goldschmidt, J. Benick, S. W. Glunz, A. W. Bett, and F. Dimroth, "Four-junction spectral beam-splitting photovoltaic receiver with high optical efficiency," *Prog. Photovoltaics*, vol. 19, pp. 61–72, Jan. 2011.

[21] N. Mohammad, P. Wang, D. J. Friedman, and R. Menon, "Enhancing photovoltaic output power by 3-band spectrum-splitting and concentration using a diffractive micro-optic," *Opt. Exp.*, vol. 22, pp. A1519–A1525, Oct. 20, 2014.

[22] J. M. Russo, S. D. Vorndran, D. Zhang, M. Gordon, Y. Wu, and R. K. Kostuk, "Grating-over-lens holographic spectrum splitting concentrating photovoltaics," presented at the Renewable Energy Environ. Conf., Tucson, AZ, USA, 2013, Paper RW1D.2.

[23] M. G. Debije and P. P. C. Verbunt, "Thirty years of luminescent solar concentrator research: solar energy for the built environment," *Adv. Energy Mater.*, vol. 2, pp. 12–35, Jan. 2012.

[24] W. G. J. H. M. van Sark, Z. Krumer, C. De Mello Donega, and R. E. I. Schropp, "Luminescent solar concentrators: The route to 10% efficiency," in *Proc. IEEE 40th Photovoltaic Spec. Conf.*, 2014, pp. 2276–2279.

[25] M. S. Kulkarni and H. F. Erk, "Acid-based etching of silicon wafers: Mass-transfer and kinetic effects," *J. Electrochem. Soc.*, vol. 147, pp. 176–188, Jan. 2000.

[26] Z. Yu, B. Wheelwright, R. Angel, and Z. C. Holman, "Silicon wafers with optically specular surfaces formed by chemical polishing," in preparation.

[27] M. F. Weber, C. A. Stover, L. R. Gilbert, T. J. Nevitt, and A. J. Ouderkirk, "Giant birefringent optics in multilayer polymer mirrors," *Science*, vol. 287, pp. 2451–2456, Mar. 31, 2000.

[28] NREL, Spectral Solar Radiation Data Base. [Online]. Available: http://rredc.nrel.gov/solar/old_data/spectral/

[29] M. A. Green, "The future of crystalline silicon solar cells," *Prog. Photovoltaics*, vol. 8, pp. 127–139, Jan./Feb. 2000.

[30] J. F. Geisz, M. A. Steiner, I. Garcia, S. R. Kurtz, and D. J. Friedman, "Enhanced external radiative efficiency for 20.8% efficient single-junction GaInP solar cells," *Appl. Phys. Lett.*, vol. 103, p. 041118, Jul. 22 2013.

[31] K. Derendorf, S. Essig, E. Oliva, V. Klinger, T. Roesener, S. P. Philipps, J. Benick, M. Hermle, M. Schachtner, G. Siefer, W. Jager, and F. Dimroth, "Fabrication of GaInP/GaAs//Si Solar cells by surface activated direct wafer bonding," *IEEE J. Photovoltaics*, vol. 3, no. 4, pp. 1423–1428, Oct. 2013.

[32] J. P. Connolly, D. Mencaraglia, C. Renard, and D. Bouchier, "Designing III-V multi-junction solar cells on silicon," *Prog. Photovoltaics*, vol. 22, pp. 810–820, Jul. 2014.

[33] P. Loper, B. Niesen, S. J. Moon, S. M. de Nicolas, J. Holovsky, Z. Remes, M. Ledinsky, F.-J. Haug, J.-H. Yum, S. De Wolf, and C. Ballif, "Organic-inorganic halide perovskites: Perspectives for silicon-based tandem solar cells," *IEEE J. Photovoltaics*, vol. 4, no. 6, pp. 1545–1551, Nov. 2014.

[34] J. W. Garland, T. Biegala, M. Carmody, C. Gilmore, and S. Sivananthan, "Next-generation multi-junction solar cells: The promise of II-VI materials," *J. Appl. Phys.*, vol. 109, p. 102423, May 15, 2011.

[35] X. Mathew, J. Drayton, V. Parikh, N. R. Mathews, X. G. Liu, and A. D. Compaan, "Development of a semitransparent CdMgTe/CdS top cell for applications in tandem solar cells," *Semiconductor Sci. Technol.*, vol. 24, p. 015012, Jan. 2009.

[36] T. J. Coutts, J. S. Ward, D. L. Young, K. A. Emery, T. A. Gessert, and R. Noufi, "Critical issues in the design of polycrystalline, thin-film tandem solar cells," *Prog. Photovoltaics*, vol. 11, pp. 359–375, Sep. 2003.

[37] D. Xu, T. Biegala, M. Carmody, J. W. Garland, C. Grein, and S. Sivananthan, "Proposed monolithic triple-junction solar cell structures with the potential for ultrahigh efficiencies using II-VI alloys and silicon substrates," *Appl. Phys. Lett.*, vol. 96, p. 073508, Feb. 15, 2010.

[38] M. A. Green, K. Emery, Y. Hishikawa, W. Warta, and E. D. Dunlop, "Solar cell efficiency tables (Version 45)," *Prog. Photovoltaics*, vol. 23, pp. 1–9, Jan. 2015.

[39] M. Carmody, S. Mallick, J. Margetis, R. Kodama, T. Biegala, D. Xu, P. Bechmann, J. W. Garland, and S. Sivananthan, "Single-crystal II-VI on Si single-junction and tandem solar cells," *Appl. Phys. Lett.*, vol. 96, p. 153502, Apr. 12, 2010.

[40] M. A. Green, K. Emery, Y. Hishikawa, W. Warta, and E. D. Dunlop, "Solar cell efficiency tables (version 42)," *Prog. Photovoltaics*, vol. 21, pp. 827–837, Aug. 2013.

[41] X. T. Wang and A. Barnett, "The effect of spectrum variation on the energy production of triple-junction solar cells," *IEEE J. Photovoltaics*, vol. 2, no. 4, pp. 417–423, Oct. 2012.

[42] A. Nakajima, M. Ichikawa, T. Sawada, M. Yoshimi, and K. Yamamoto, "Spectral characteristics of thin-film stacked-tandem solar modules," *Japanese J. Appl. Phys. Part 1*, vol. 43, pp. 7296–7302, Oct. 2004.

[43] T. M. Pavlovic, I. S. Radonjic, D. D. Milosavljevic, and L. S. Pantic, "A review of concentrating solar power plants in the world and their potential use in Serbia," *Renewable Sustainable Energy Rev.*, vol. 16, pp. 3891–3902, Aug. 2012.

[44] *FOA: Full-spectrum Optimized Conversion and Utilization of Sunlight (FOCUS)*, ARPA-E, Washington, DC, USA, 2013.

[45] A. Mills and R. Wiser, "Changes in the economic value of variable generation at high penetration levels: A pilot case study of California," Lawrence Berkeley Nat. Lab., Berkeley, CA, USA, Rep. LBNL-6182E, 2012.

[46] D. Barlev, R. Vidu, and P. Stroeve, "Innovation in concentrated solar power," *Sol. Energy Mater. Sol. Cells*, vol. 95, pp. 2703–2725, Oct. 2011.

[47] J. Blanco, S. Malato, P. Fernandez-Ibanez, D. Alarcon, W. Gernjak, and M. L. Maldonado, "Review of feasible solar energy applications to water processes," *Renewable Sustainable Energy Rev.*, vol. 13, pp. 1437–1445, Aug./Sep. 2009.

Authors' photographs and biographies not available at the time of publication.